



**OAK RIDGE
NATIONAL
LABORATORY**

MARTIN MARIETTA

**Confinement Improvement of
Low-Aspect-Ratio Torsatrons**

B. A. Carreras
V. E. Lynch
N. Dominguez
J. N. Leboeuf
J. F. Lyon

OAK RIDGE NATIONAL LABORATORY
CENTRAL RESEARCH LIBRARY
CIRCULATION SECTION
ROOM 1008 113
LIBRARY LOAN COPY
DO NOT TRANSFER TO ANOTHER PERSON
If you wish someone else to see this
report, send in name with report and
the library will arrange a loan.

OPERATED BY
MARTIN MARIETTA ENERGY SYSTEMS, INC.
FOR THE UNITED STATES
DEPARTMENT OF ENERGY

ORNL/TM-11101
Dist. Category UC-427

Fusion Energy Division

**CONFINEMENT IMPROVEMENT OF
LOW-ASPECT-RATIO TORSATRONS**

B. A. Carreras

V. E. Lynch*

N. Dominguez

J. N. Leboeuf

J. F. Lyon

*Computing and Telecommunications Division, Martin Marietta Energy Systems, Inc.

DATE PUBLISHED: March 1989

Prepared by the
OAK RIDGE NATIONAL LABORATORY
Oak Ridge, Tennessee 37831
operated by
MARTIN MARIETTA ENERGY SYSTEMS, INC.
for the
U.S. DEPARTMENT OF ENERGY
under contract DE-AC05-84OR21400



3 4456 0290433 8

CONTENTS

ABSTRACT	v
1. INTRODUCTION	1
2. ISSUES FOR LOW-ASPECT-RATIO STELLARATORS	3
3. OPTIMIZATION CRITERIA	4
4. LOW-ASPECT-RATIO TORSATRON CONFIGURATIONS WITH IMPROVED CONFINEMENT	13
5. DISCUSSION AND CONCLUSIONS	21
ACKNOWLEDGMENT	23
REFERENCES	25

ABSTRACT

Stellarators with plasma aspect ratios in the range from 3.5 to 5 can be created using the Compact Torsatron configurations. Stable operation at high beta should be possible in these devices if a vertical field coil system is designed to prevent breaking of the magnetic surfaces at finite beta. Direct losses of energetic particles can be high, but the addition of an external quadrupole field can reduce these losses. Optimization criteria and the low-aspect-ratio torsatron configurations obtained are discussed.

1. INTRODUCTION

Stellarators traditionally have been considered large-aspect-ratio configurations. In recent years, interest in low-aspect-ratio stellarator configurations has increased.¹⁻⁷ Many configurations are being studied, and some of the new experiments have plasma aspect ratios, $A_p = R_0/\bar{a}$, of <10 . A motivating factor in these studies is to move toward a more compact stellarator that could result in a competitive ignited stellarator device and, in the long run, lead to a more attractive fusion reactor.^{8,9} However, as yet there is no experiment in the very small aspect ratio range; such an experiment could resolve some of the critical issues for these configurations and provide a data base for future optimization of aspect ratio. Here we present some assessment studies directed toward defining such an experiment.

The strategy followed in the present configuration studies has three basic components: (1) to define simple theoretical criteria that can be applied to vacuum fields and permit an evaluation of the main physics properties relevant to low-aspect-ratio stellarator configurations; (2) to look for ways of experimentally testing these criteria in present experiments; and (3) to use the Advanced Toroidal Facility (ATF) configuration as a reference case in the sense of maintaining its physics properties while we try to reduce its aspect ratio.

In the calculations described here, we start by defining a coil set and use these coils to modify the fields on the basis of what we learn from the theoretical criteria. We take this approach because most of the numerical tools that we use have been developed from this point of view. This also allows us to go on using the continuous helical coils that were a key feature in our stellarator reactor studies.⁹ The main problem of such an approach is to find a magnetic field configuration with good magnetic surfaces that is close to the configuration that satisfies the theoretical criteria. The method developed by Cary and Hanson¹⁰ for reconstruction of flux surfaces offers a solution to this problem. An initial assessment of low-aspect-ratio torsatrons following this method was presented in Ref. 4. There, the application of the Cary-Hanson method to this type of study was described. However, the study presented in Ref. 4 took into consideration only magnetohydrodynamic (MHD) constraints. Here, we present a more general study by including both MHD and transport constraints in the configuration evaluation. Some of the results discussed here were presented at the 12th International Conference on Plasma Physics and Controlled Nuclear Fusion Research.⁶ An alternative systematic approach that does

not require magnetic surface reconstruction for low-aspect-ratio torsatron optimization is discussed in Ref. 11.

The criteria derived in this paper are rather simple so that they can be used in analysis of vacuum magnetic fields. They do not guarantee that the selected configurations will have all the properties desired. These configurations must be tested a posteriori for their equilibrium, stability, and transport properties. However, in practice these criteria have worked fairly well, and the subsequent detailed physics studies have generally confirmed the initial assessment. We have used the criteria to find low-aspect-ratio torsatrons with plasma aspect ratios in the range from 3.5 to 5 and physics properties close to those of ATF.

This paper is organized in the following way. In Sect. 2, we discuss the main issues for low-aspect-ratio stellarators. The associated theoretical criteria are derived in Sect. 3. The configurations resulting from these studies are presented in Sect. 4, and a discussion of the results and our conclusions are given in Sect. 5.

2. ISSUES FOR LOW-ASPECT-RATIO STELLARATORS

The main physics issues for low-aspect-ratio stellarators can be summarized in the following points:

- **Magnetic surface fragility.** At low aspect ratio, the $1/R$ helical-symmetry-breaking terms are important. In vacuum, they cause the loss of outer magnetic surfaces. At finite beta, the beta-induced magnetic axis shift increases the size of the symmetry-breaking terms¹² in such a way that they can severely limit the achievable beta in a given device.
- **Equilibrium beta limit.** The equilibrium beta limit for classical stellarators scales as $\beta_c \sim \iota^2/A_p \propto A_p$. Therefore, reducing the aspect ratio can cause a decrease in the beta limit. This issue is coupled to the previous one because the fragility of the outer magnetic surfaces is what limits the edge rotational transform $\iota(\bar{a})$ achievable at low aspect ratio.
- **Energetic particle confinement.** The alpha particle confinement, or the confinement of any energetic particle tail, is strongly affected by the field ripple. Loss of energetic particles is not expected to be healed by the electric field effects that contribute to the confinement of thermal particles. For stellarators, the relevant ripple is $\epsilon_t = 1/A_p$, which, of course, increases at low aspect ratio.
- **Transport in the low collisionality regime.** A main concern for stellarator confinement is diffusive losses in the $1/\nu$ regime,¹³ which are not affected by the electric field. The particle flux in the $1/\nu$ regime has been calculated in Ref. 14 for a multiple-helicity stellarator. When only toroidal ripple, ϵ_t , and helical ripple, ϵ_h , are considered, the particle flux in the $1/\nu$ regime scales as $\epsilon_h^{3/2} \epsilon_t^2$. Therefore, the losses in the $1/\nu$ regime increase at least as fast as A_p^{-2} .
- **Bootstrap current.** The bootstrap current can be a problem for zero-net-current stellarator operation at low collisionality, independent of the aspect ratio, because plasma currents can modify the desired rotational transform profile, leading to instabilities.
- **Stability.** In general, stability is not an issue at low aspect ratio except when one tries to modify the magnetic configuration to improve confinement.

We have concentrated our attention on these physics issues. In Sect. 3, we define simple criteria for optimization of the vacuum fields that address each of these issues.

3. OPTIMIZATION CRITERIA

We consider the criteria in the same order as the issues listed in Sect. 2.

1. **Magnetic surface fragility.** For very low aspect ratio stellarator configurations, magnetic surface fragility is a critical issue. At low aspect ratio, it is not enough to have an accurate design for the coils, because small shifts of the magnetic axis can cause serious destruction of the outer surfaces. A possible solution to this problem, proposed in Ref. 4, is to use an axisymmetric coil system to control the magnetic surfaces at finite beta. It is necessary to have active control through feedback on the value of beta. Although numerical calculations show that this method can work, an experimental test in a very low aspect ratio stellarator is desirable. For the purpose of the calculations presented here, we assume that the method works and that we can maintain the outer flux surface of a stellarator at any beta value.
2. **Equilibrium beta limit.** Once we assume that magnetic surface control is practical, the question of the equilibrium beta limit in a stellarator can be viewed from a different perspective. In a stellarator, the equilibrium beta limit is conventionally given by $\beta_c \sim \iota^2/A_p$. In a classical torsatron, to avoid the breaking of magnetic surfaces, the helical winding pitch cannot be varied significantly from a standard value; this condition implies that the rotational transform is proportional to A_p . Therefore, the equilibrium beta limit for a classical torsatron scales with aspect ratio as $\beta_c \propto A_p$. However, if active control of magnetic surfaces is successful, one can maintain $\iota(\bar{a})$ at a constant value when the aspect ratio is changed. In this case, the equilibrium beta limit scales with aspect ratio as $\beta_c \propto A_p^{-1}$, like that in tokamaks. Therefore, to maintain the equilibrium-beta limit properties of ATF in looking for low-aspect-ratio configurations, we set

$$\iota(\bar{a}) \approx 1.0 \tag{C1}$$

as the first of our criteria.

3. **Energetic particle confinement.** The main problem in this area is the confinement of the helically trapped particles. Low-aspect-ratio torsatrons have a relatively large population of helically trapped particles. For $A_p < 5$, essentially all the energetic trapped particles are lost, down to energies of two to three times the thermal energy.¹⁵ For alpha particles in a minimum-size reactor or for the high-energy tail of a next-generation experiment, this loss corresponds to about 50% of the trapped particles, or 15% of the total, at $A_p = 8$ ($M = 12$,

with M the number of field periods) and 100% of the trapped particles, or 35% of the total, at $A_p = 4$ ($M = 6$). The Fokker-Planck equation has been used in calculating the loss of initially confined alpha particles that scatter into the trapped particle loss region; these calculations show an additional energy loss of about 15%. Because the indirect losses are weaker functions of the configuration parameters, we focus our optimization study on the minimization of the direct losses. If the direct trapped particle orbit losses can be eliminated, the indirect losses also disappear. The deeply trapped particles closely follow, in a bounce-averaged sense, surfaces of constant $q\Phi_E + \mu B_{\min}$. Here, q is the charge of the particle in the electrostatic potential Φ_E , μ is the magnetic moment, and $B_{\min} = \min_{\zeta} |\vec{B}(\psi, \theta, \zeta)|$ with (ψ, θ, ζ) the Boozer coordinates;¹⁶ ψ is the toroidal flux divided by 2π , and θ and ζ are the poloidal and toroidal angles in this coordinate system. For energetic particles, electric field effects are not important, and the $B_{\min} = \text{const}$ surfaces give a good indication of the deeply trapped particle orbit topology.¹⁷ A way to visualize the orbit topology is to plot the contours of constant $B_{\min}(\psi, \theta)$ in the plane $(\sqrt{\psi} \cos \theta, \sqrt{\psi} \sin \theta)$, as is done in Fig. 1 for the standard ATF configuration. In this representation, the magnetic flux surfaces are shown as concentric circles. We have plotted the circles corresponding to the last flux surface (taken to be the plasma boundary) and to the flux surface with an average radius half that of the average plasma radius. This plot clearly indicates the departure of the deeply trapped particle orbits from the flux surfaces. The fractional area enclosed by the last closed B_{\min} contour correlates with the fraction of trapped particles confined.^{5,15} Therefore, the value of this area, A_B , is useful in assessing the energetic particle confinement properties of a magnetic configuration.¹⁷ From the studies in Ref. 15 of the correlation between A_B and the trapped particle loss, it is clear that to cause any significant increase of the fraction of trapped particles confined, A_B must be larger than 0.4. Therefore, we take as a criterion for energetic particle confinement

$$0.4 < A_B . \quad (\text{C2})$$

The effectiveness of this criterion can be tested in ATF. By changing the dipole and/or the quadrupole component of the vertical field, we can change A_B considerably, as shown in Fig. 2. In Fig. 3, we plot the average magnetic surfaces for ATF with the same VF coil currents used in Fig. 2. Decreasing the mid-VF

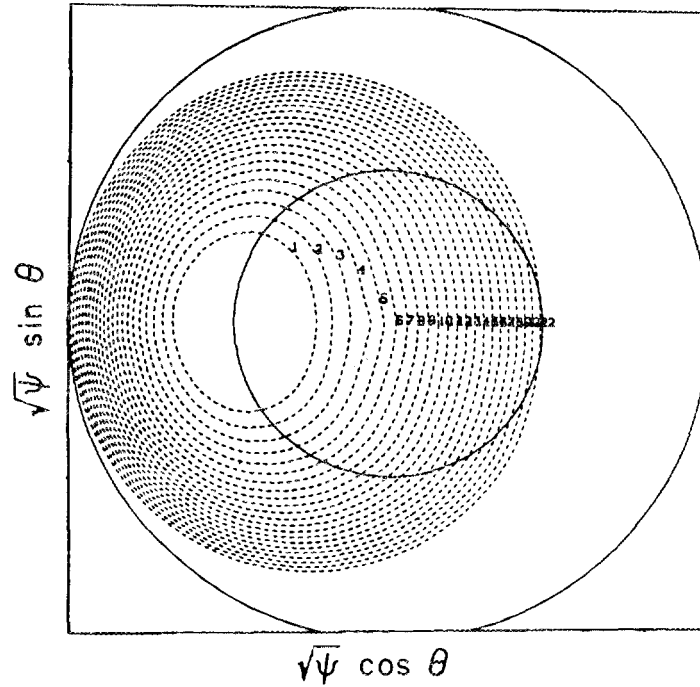


FIG. 1. Plot of the minimum- B contours for the ATF standard configuration in the plane $(\sqrt{\psi} \cos \theta, \sqrt{\psi} \sin \theta)$. The circles are the $\psi = 1$ and $\psi = 0.25$ flux surfaces.

coil current I (which is related to the quadrupole moment of the poloidal field) increases A_B and decreases the plasma ellipticity. Decreasing R_0 (shifting the major axis inward, thus changing the dipole moment of the poloidal field) also increases A_B . However, because an inward shift of the magnetic axis is not always compatible with plasma stability, the possibility of using the quadrupole field component to increase A_B is particularly interesting.

4. **Transport in the low collisionality regime** (in particular, in the $1/\nu$ regime). The calculation of Shaing and Hokin¹⁴ for a multiple-helicity magnetic field, which they parameterize as

$$|\vec{B}| = B_0 \left[1 + \epsilon_t \cos \theta + \epsilon_d \cos \ell \theta + \sum_{n=-\infty}^{\infty} \epsilon^{(n)} \cos(n\theta + M\zeta) \right],$$

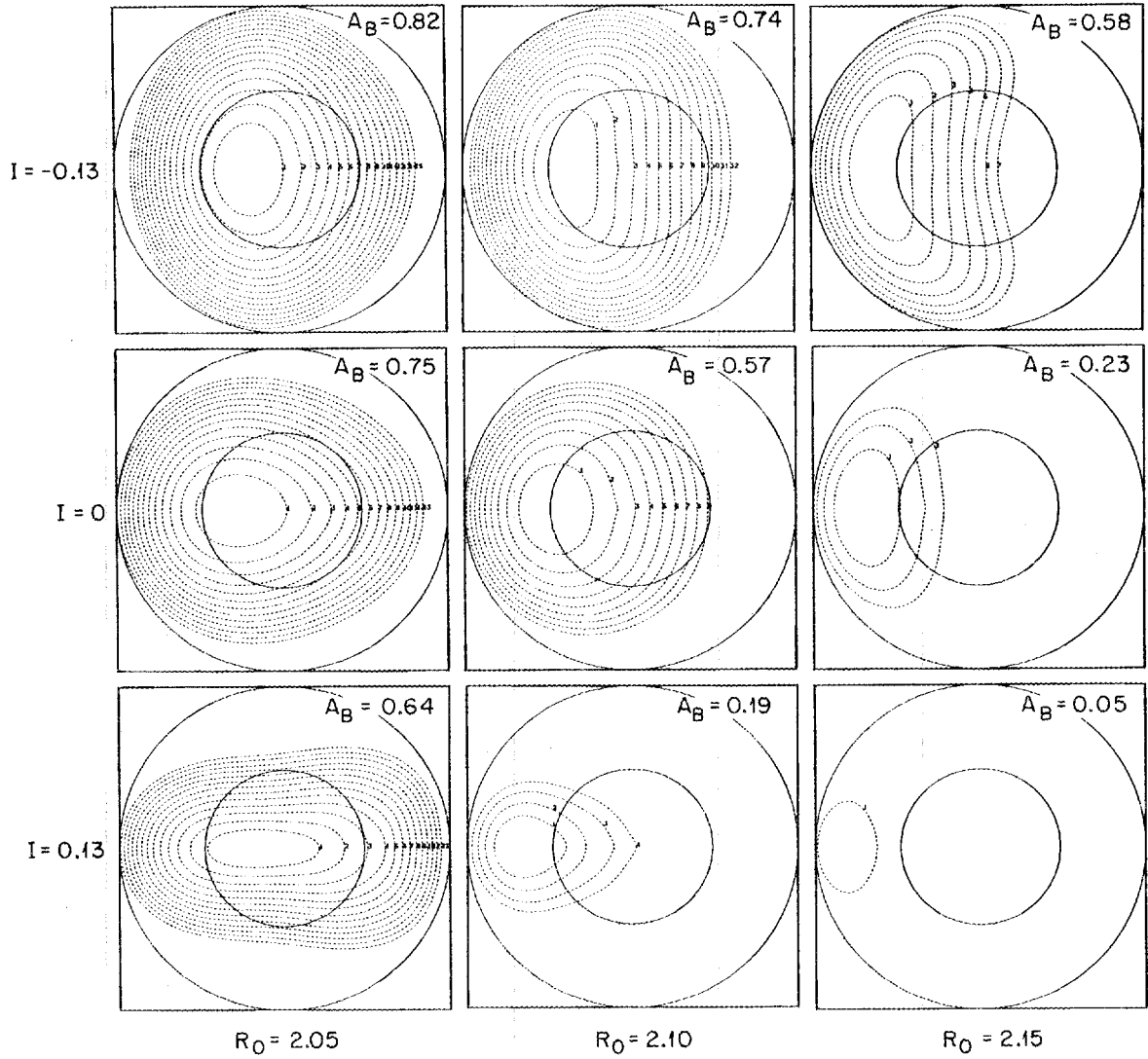


FIG. 2. Effect of the dipole (R_0 shift) and quadrupole (I) components of the ATF poloidal field on the minimum- B contours.

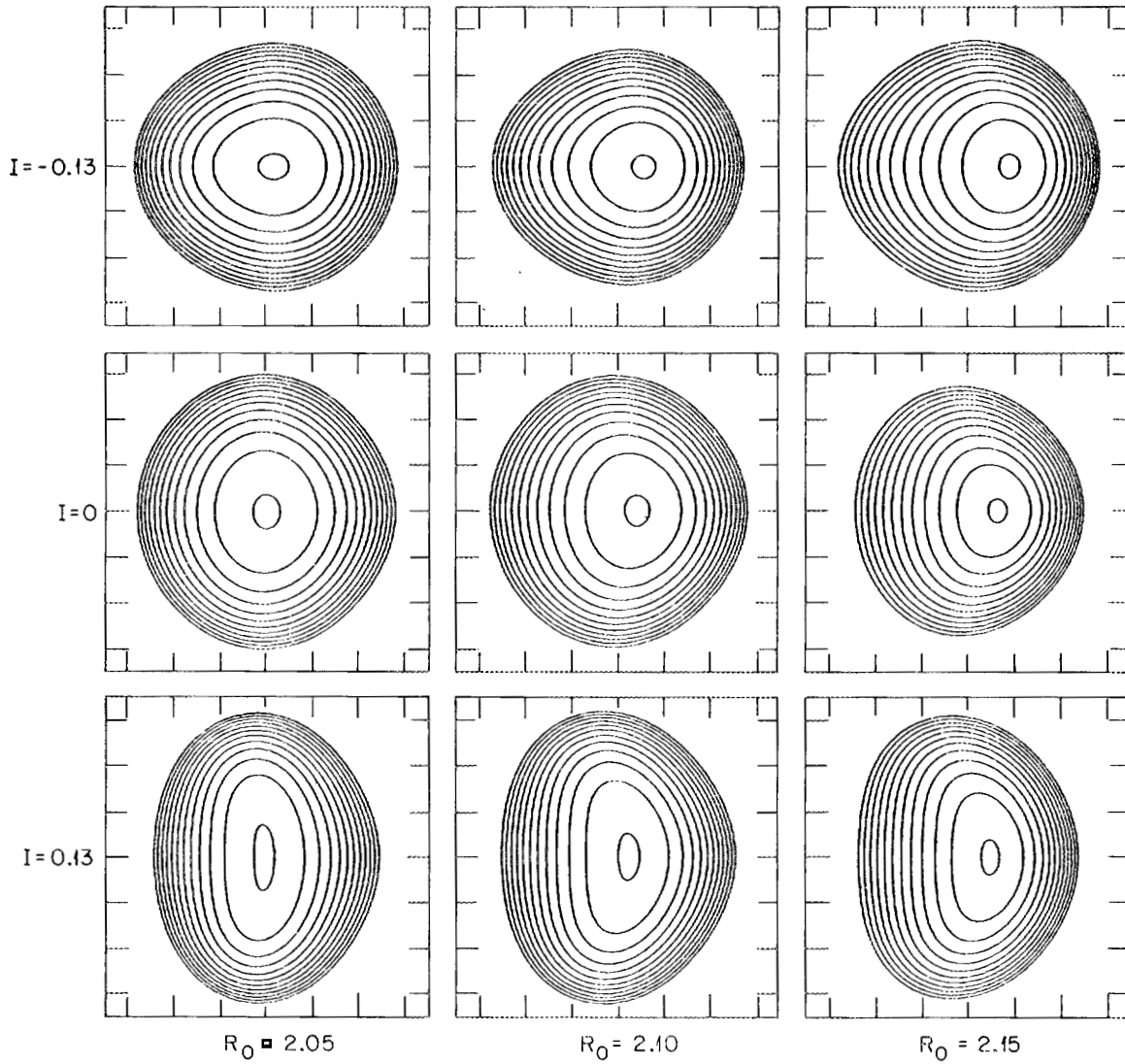


FIG. 3. Effect of the dipole and quadrupole components of the ATF poloidal field on the vacuum-field average magnetic surfaces.

yields the geometrical factor in the particle flux

$$\Gamma = \int_0^{2\pi} d\theta \epsilon_H(\theta)^{3/2} \left[G_1 \left(\frac{\partial \epsilon_T}{\partial \theta} \right)^2 - 2G_2 \frac{\partial \epsilon_T}{\partial \theta} \frac{\partial \epsilon_H}{\partial \theta} + G_3 \left(\frac{\partial \epsilon_H}{\partial \theta} \right)^2 \right] .$$

Here $\epsilon_T(\theta)$ and $\epsilon_H(\theta)$, the effective toroidal and helical ripple, respectively, are functions of θ and of the coefficients ϵ_t , ϵ_d , and $\epsilon^{(n)}$, and the G_i ($i = 1, 2, 3$) are numerical coefficients. Explicit expressions for these functions and coefficients are given in Ref. 14. By changing the magnetic field components of $|\vec{B}|$, it is possible to change the particle flux. Using the quadrupole field component, we can change the value of Γ for ATF by more than a factor of 5 (Fig. 4). Not surprisingly, the effect of the quadrupole field component goes in the same direction as the improvement of the energetic particle confinement. If Γ_{ATF} is the value of the geometrical factor in the particle flux in the $1/\nu$ regime for the ATF standard configuration, we use as a criterion in searching for low-aspect-ratio configurations

$$\Gamma \lesssim \Gamma_{\text{ATF}} . \quad (\text{C3})$$

5. **Bootstrap current.** An expression for the bootstrap current for a three-dimensional (3-D) system with nested magnetic surfaces was derived in Ref. 18. The expression is similar to that for an axisymmetric case with a geometrical factor G_b that depends only on the components of $|\vec{B}|$. This geometrical factor G_b is 1 for tokamaks and <1 for stellarators. By using added magnetic field components (i.e., dipole, quadrupole) or by giving a slight helical axis to the configuration, the geometrical factor can be set to practically zero, as discussed in detail in Ref. 19. The criterion we adopt for our configuration studies is

$$G_b \approx 0 . \quad (\text{C4})$$

In Ref. 19, it was also shown that this criterion could be tested experimentally in ATF.

6. **Stability.** For low-aspect-ratio torsatrons, such as ATF, the main stabilization mechanisms are the magnetic well at the plasma center and shear at the edge. This combination of stabilization mechanisms produces a beta self-stabilization effect²⁰ that leads to a high-beta second stability regime for these configurations.⁴ To guarantee a magnetic well at finite beta, a minimum requirement is

$$V''(0) < 0 . \quad (\text{C5})$$

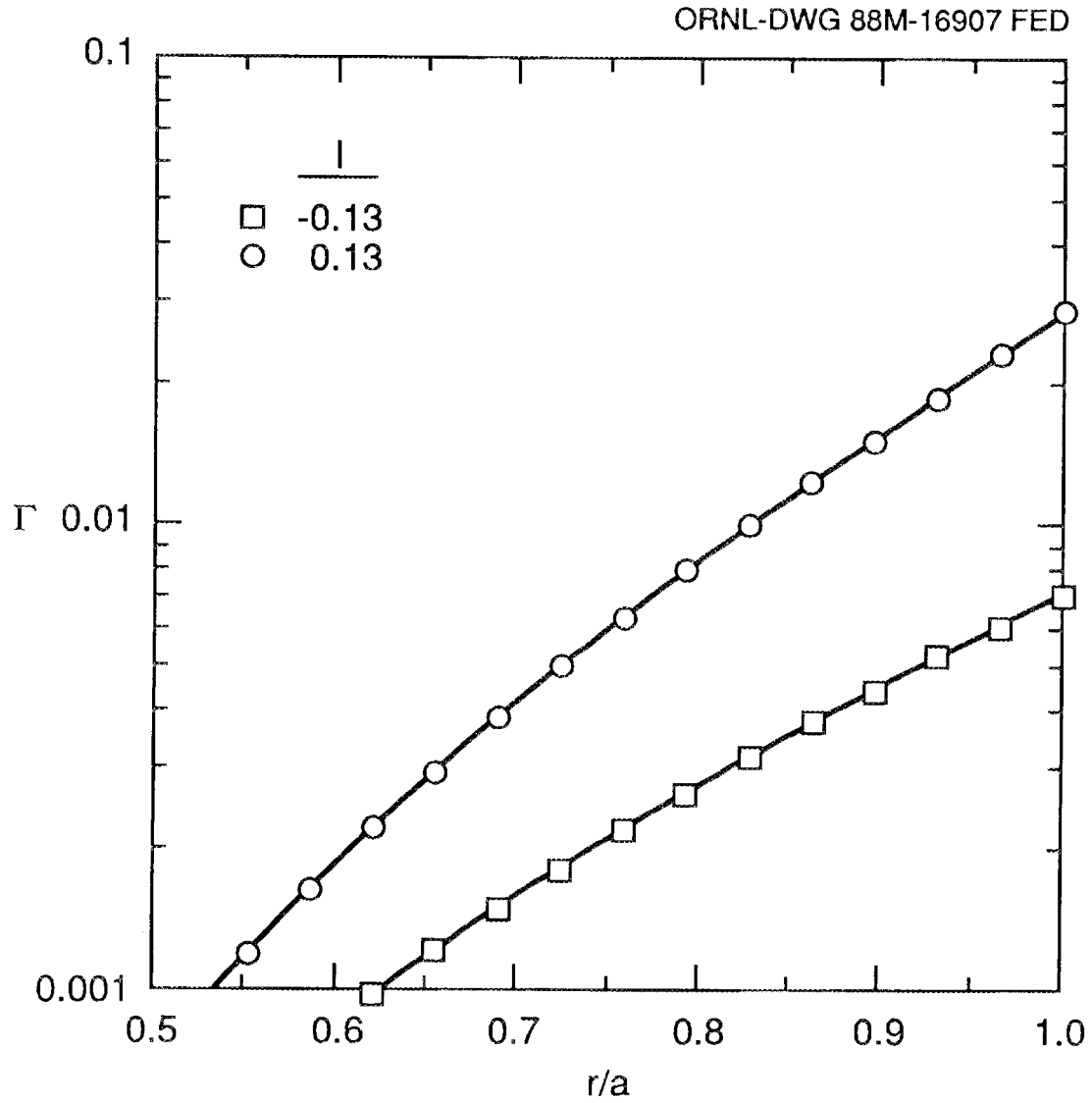


FIG. 4. Effect of the quadrupole component I of the ATF poloidal field on the geometrical factor in the particle flux for the $1/\nu$ regime.

In some cases, we have used the stronger requirement of $V'' < 0$ at the $r = 1/2$ surface. However, it is not always necessary to be so stringent. To have enough shear over the whole plasma volume, we require

$$\epsilon(0) < 0.4 . \quad (\text{C6})$$

These criteria were applied in our first optimization studies, which were focused only on achieving stable high-beta operation.⁴ However, when we include the transport and energetic particle confinement constraints, criteria (C5) and (C6) are not enough to guarantee stability. We must also impose a condition on the geodesic curvature term if we want to maintain the beta self-stabilization condition. The beta self-stabilization effect is caused by the β^2 term in the Mercier criterion.²¹ The sum of the terms must be positive overall; that is, the magnetic well effects must dominate over the geodesic curvature terms. For zero-current equilibria, a sufficient condition is

$$\left(V'' - V_v'' \right) \frac{dp}{ds} - \int \int g \frac{d\theta}{B^2} \frac{d\zeta}{ds} \left(\frac{dp}{ds} \right)^2 - \int \int g \frac{d\theta}{g^{ss}} \frac{d\zeta}{B^2} (\vec{J} \cdot \vec{B})^2 > 0 .$$

Here, g is the Jacobian, p is the pressure, s is the toroidal flux, and $g^{ss} \equiv |\vec{\nabla}s|^2$ is the corresponding metric element. The primes indicate derivatives with respect to s , and V_v'' is V'' for the vacuum field. From this condition, we can derive a bound for the ratio of the Pfirsch-Schlüter current to the diamagnetic current:

$$\frac{\langle J_{\parallel}^2 \rangle}{\langle |\vec{J}_{\perp}|^2 \rangle} \equiv \left[\int \int g \frac{d\theta}{g^{ss}} \left(\frac{\vec{J} \cdot \vec{B}}{B} \right)^2 \right] / \left(\int \int g \frac{d\theta}{g^{ss}} |\vec{J}_{\perp}|^2 \right) ,$$

given by

$$\frac{\langle J_{\parallel}^2 \rangle}{\langle |\vec{J}_{\perp}|^2 \rangle} < \frac{4\epsilon_t}{\beta_0} \frac{\Delta_p(0)}{\bar{a}} \left(\frac{1}{\Delta_p(0)} \frac{d\Delta_p}{ds} \right) / \left(\frac{1}{p(0)} \frac{dp}{ds} \right) ,$$

where Δ_p is the magnetic axis shift with beta, and $\beta_0 = p(0)/(B_0^2/2\mu_0)$ is the peak beta. This sufficient condition is very strict. We have found that for practical purposes of analyzing the vacuum magnetic fields and for the parameter range that we consider, the simpler criterion

$$\left(\frac{\langle J_{\parallel}^2 \rangle}{\langle |\vec{J}_{\perp}|^2 \rangle} \right)^{1/2} < 6 \quad (\text{C7})$$

is adequate.

The seven criteria listed here have been used in the present configuration studies. We have proceeded as follows. First, we use the Cary-Hanson technique to construct a low-aspect-ratio configuration by minimizing the residue of the periodic field lines, using as parameters the winding law parameters α_n , the toroidal angle

$$\phi = \phi_0 + \ell \left[\theta - \sum_n \alpha_n \sin(n\theta) \right] / M ,$$

and the coil minor radius a_c . Here, θ is the poloidal angle, and $\ell = 2$ for the configurations considered. The minimization is done with the constraints $\iota(0) < 0.4$ and $V''(0) < 0$, and we proceed until we achieve $\iota(\bar{a}) \approx 1$. Second, we analyze the resulting vacuum field configuration to test its compliance with the remaining criteria, (C2)–(C4) and (C7). Then we modify the quadrupole moment of the poloidal field or some other field component to improve the agreement with these criteria and reconstruct the magnetic surfaces. The process is iterated as many times as needed. Some configurations selected in this way were studied in detail to evaluate their 3-D equilibrium properties, Mercier and low- n mode stability, and energetic orbit confinement. The results are discussed in Sect. 4.

4. LOW-ASPECT-RATIO TORSATRON CONFIGURATIONS WITH IMPROVED CONFINEMENT

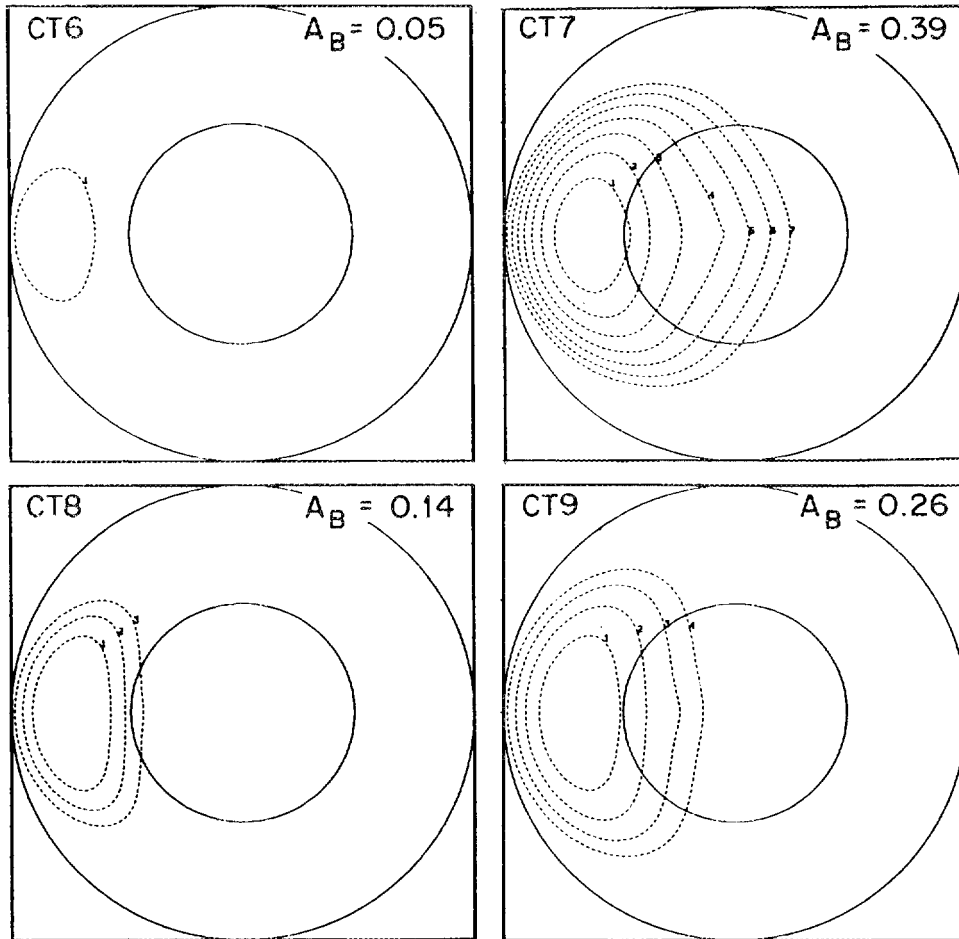
The starting point of our studies was the low-aspect-ratio torsatron configuration sequence discussed in Ref. 4. These configurations are dubbed Compact Torsatron (CT) configurations, and their parameters are summarized in Table I. In the table, $\langle\beta_c\rangle$ is the volume-average beta at the equilibrium limit, where the equilibrium limit is defined as the point at which the average magnetic axis shift is half the average plasma radius. These configurations were generated on the basis of the MHD criteria, (C1), (C5), and (C6), only. When the transport-related criteria were evaluated for these configurations, they indicated that the confinement was very poor. Practically all of the helically trapped particles were lost (Fig. 5), since all of the configurations had $A_B < 0.4$. Similarly, the geometrical factor associated with the particle flux in the $1/\nu$ regime was clearly larger for these configurations than it was for ATF (Fig. 6) and increased faster than ϵ_t^2 because ϵ_h had to be increased at the same time as ϵ_t in order to reconstruct the outer magnetic surfaces at low aspect ratio.

The addition of a quadrupole field that enhances the horizontal ellipticity of the flux surfaces in ATF also increases A_B (Fig. 2). We applied the same kind of quadrupole field to the low-aspect-ratio torsatrons, as shown in Fig. 7 for the CT9 configuration. The quadrupole field intensity is denoted by the current I

**Table I. Parameters of Compact Torsatron
sequence and ATF device**

	Configuration				
	CT6	CT7	CT8	CT9	ATF
M	6	7	8	9	12
A_p	3.8	3.3	4.2	4.8	7.8
$\langle\beta_c\rangle$ (%)	9.8	7.5	6	7	5

ORNL-DWG 89-2309 FED

FIG. 5. Minimum- B contours for the sequence of Compact Torsatrons (Table I).

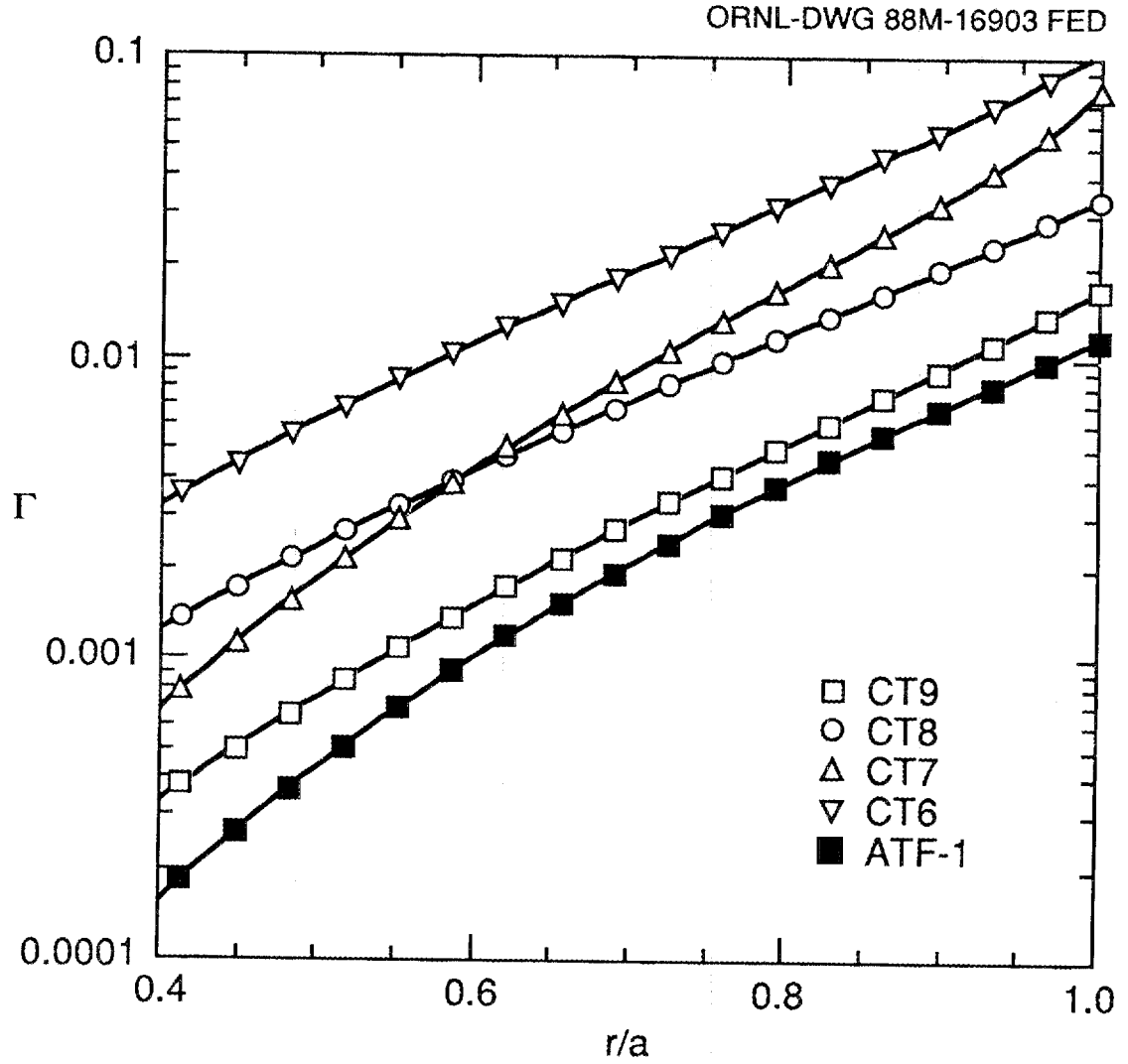


FIG. 6. Geometrical factor in the particle flux for the $1/\nu$ regime versus average radius for the Compact Torsatron sequence (Table I). ATF-1 is the standard ATF configuration.

ORNL-DWG 89-2310 FED

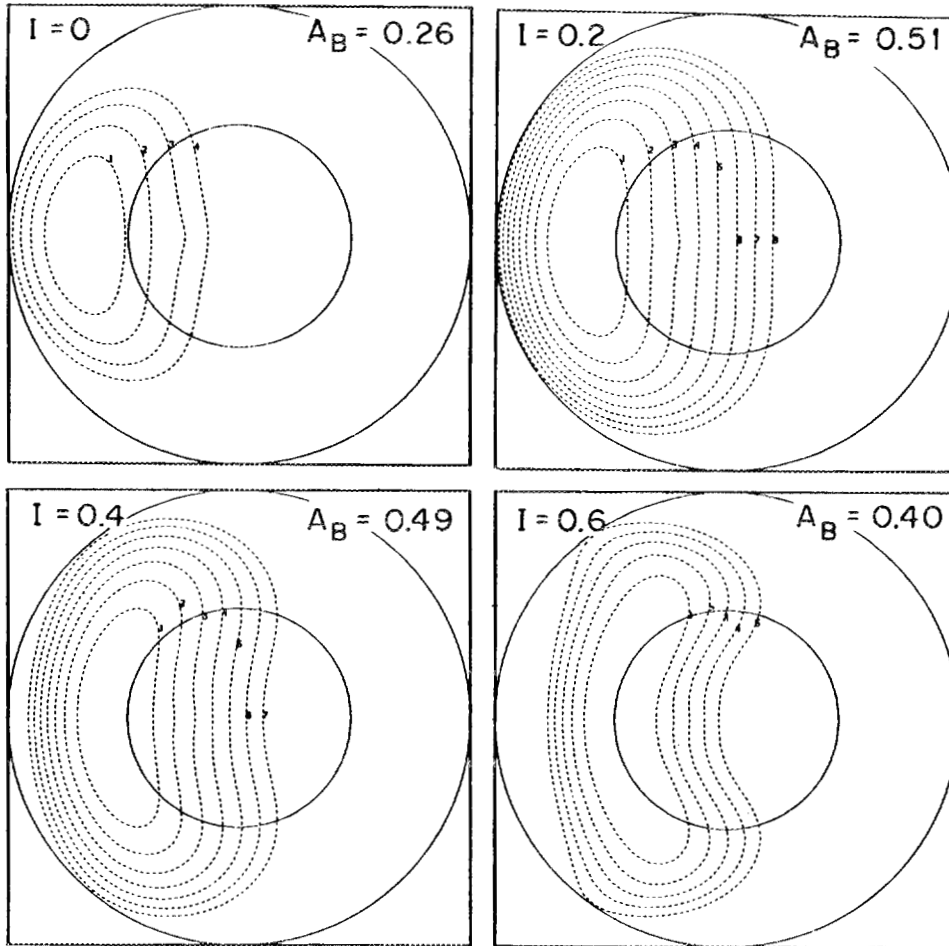


FIG. 7. Effect of an added quadrupole field on the minimum- B contours for the CT9 configuration.

in the VF coils needed to create it, normalized to the current in the helical coils. There is a marked increase in A_B for small values of the applied field; however, there is a maximum value for the quadrupole field beyond which A_B does not increase. The quadrupole field decreases the value of Γ , as shown in Fig. 8. For the CT9 configuration and for the value of the quadrupole field at which A_B is near maximum ($A_B \approx 0.5$), we can have $\Gamma_{CT9} \approx \Gamma_{ATF}$; criteria (C2) and (C3) are simultaneously satisfied for $I = -0.4$. For this value of the quadrupole field, the normalized parallel current (Fig. 9) is very close to the bound given by (C7), and the

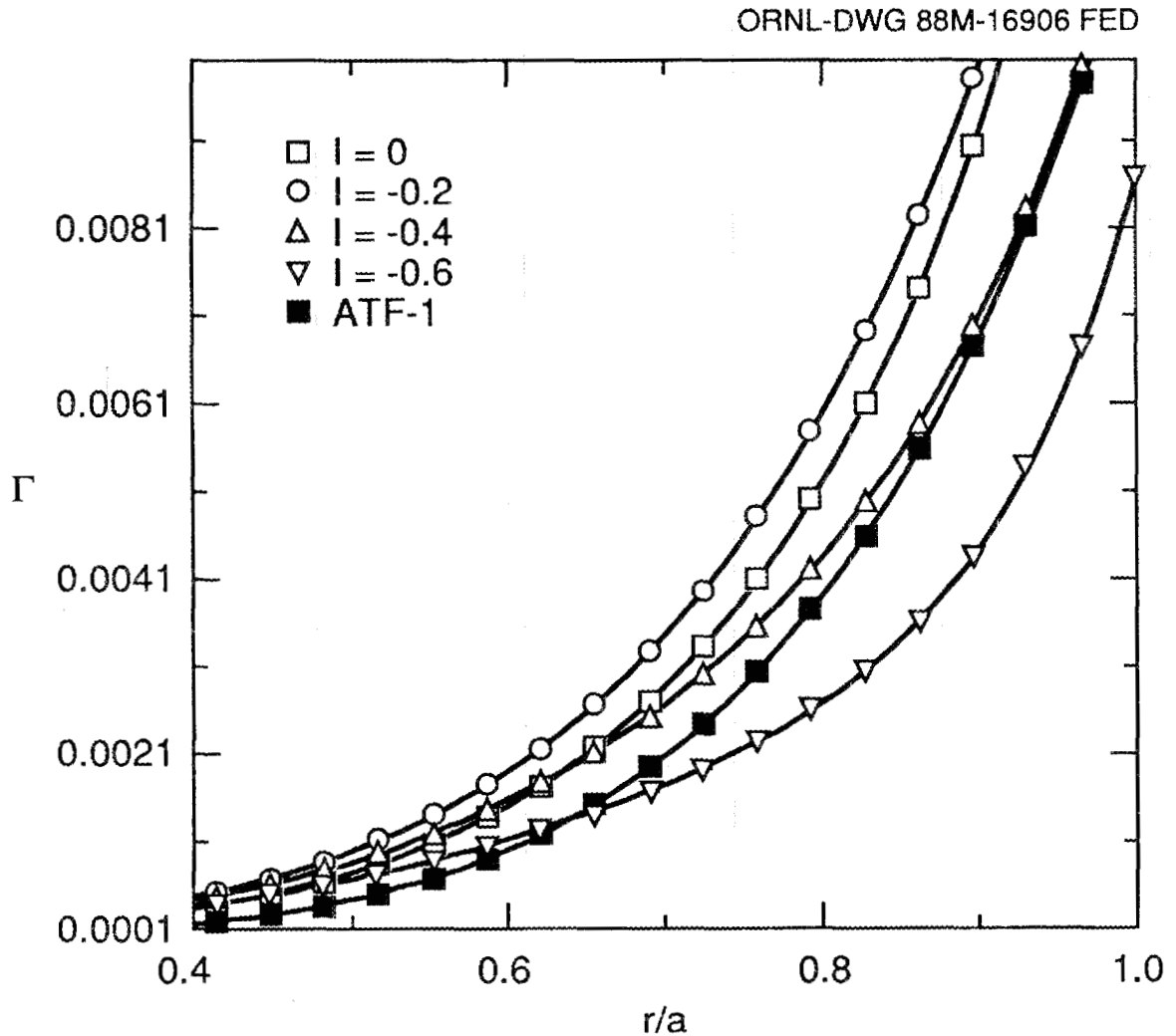


FIG. 8. Effect of an added quadrupole field on the geometrical factor Γ in the $1/\nu$ particle flux for the CT9 configuration. The Γ factor for the ATF standard configuration is plotted for comparison.

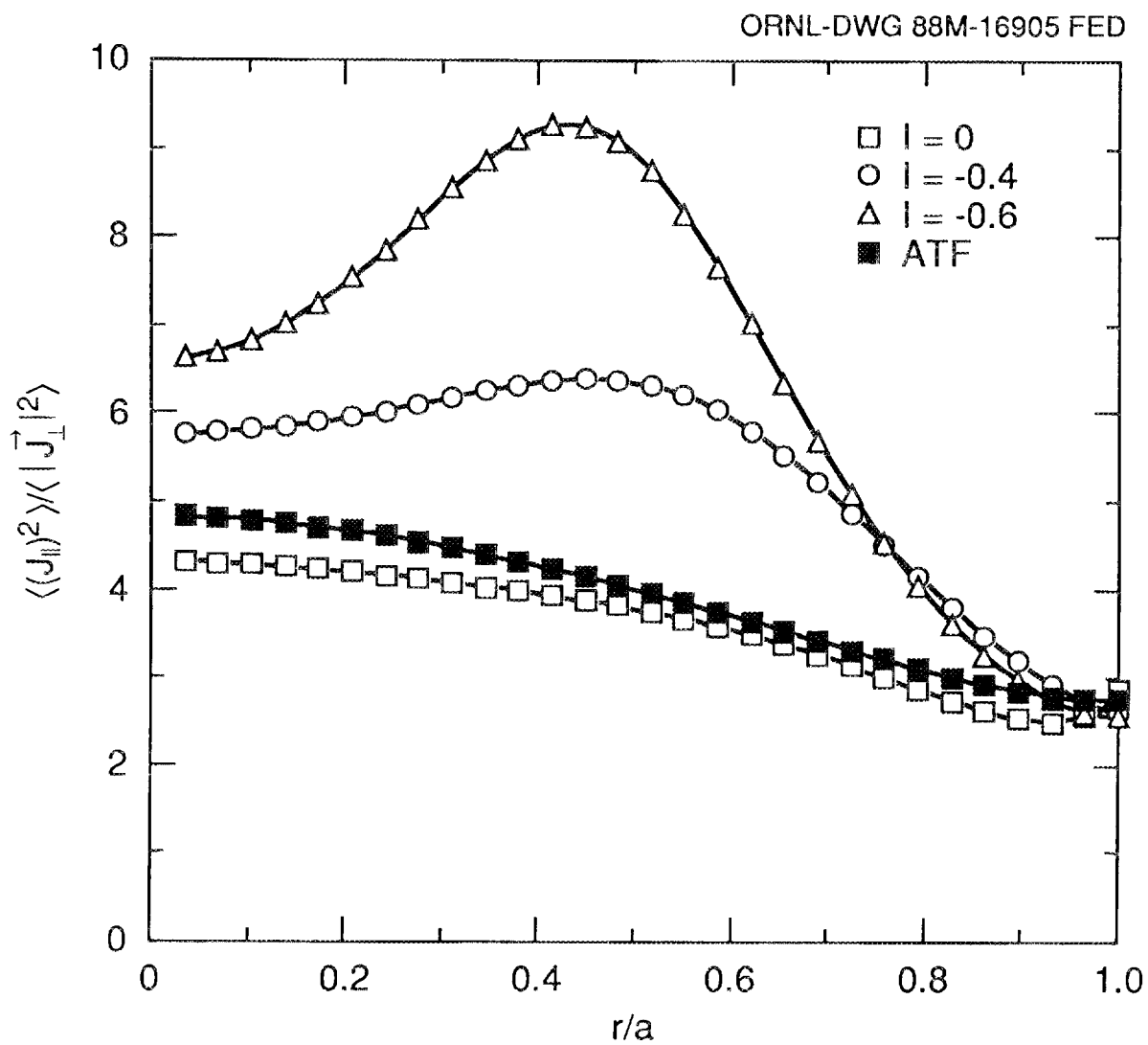


FIG. 9. Effect of an added quadrupole field on $\langle (J_{\parallel})^2 \rangle^{1/2} / \langle |\vec{J}_{\perp}|^2 \rangle^{1/2}$ for the CT9 configuration. The value for the ATF standard configuration is plotted for comparison.

stability properties are maintained. The trade-off has been in the equilibrium beta limit, which is somewhat lower than for the original CT9 configuration, $\beta_c \simeq 6\%$ ($\beta_0 \simeq 13.5\%$) compared with $\beta_c \simeq 7\%$ ($\beta_0 \simeq 16.2\%$), as shown in Fig. 10. The 3-D MHD calculations were carried out with the VMEC code.²² Magnetic surfaces for the $M = 9$ configuration with the added quadrupole field ($I = -0.4$) and for $\beta_0 = 4.3\%$ are shown in Fig. 11. Similar improvements in transport properties have been obtained for two other CT configurations, CT8 and CT7. However, for the CT6 case, we have been unable to reduce the energetic particle losses to a significant extent.

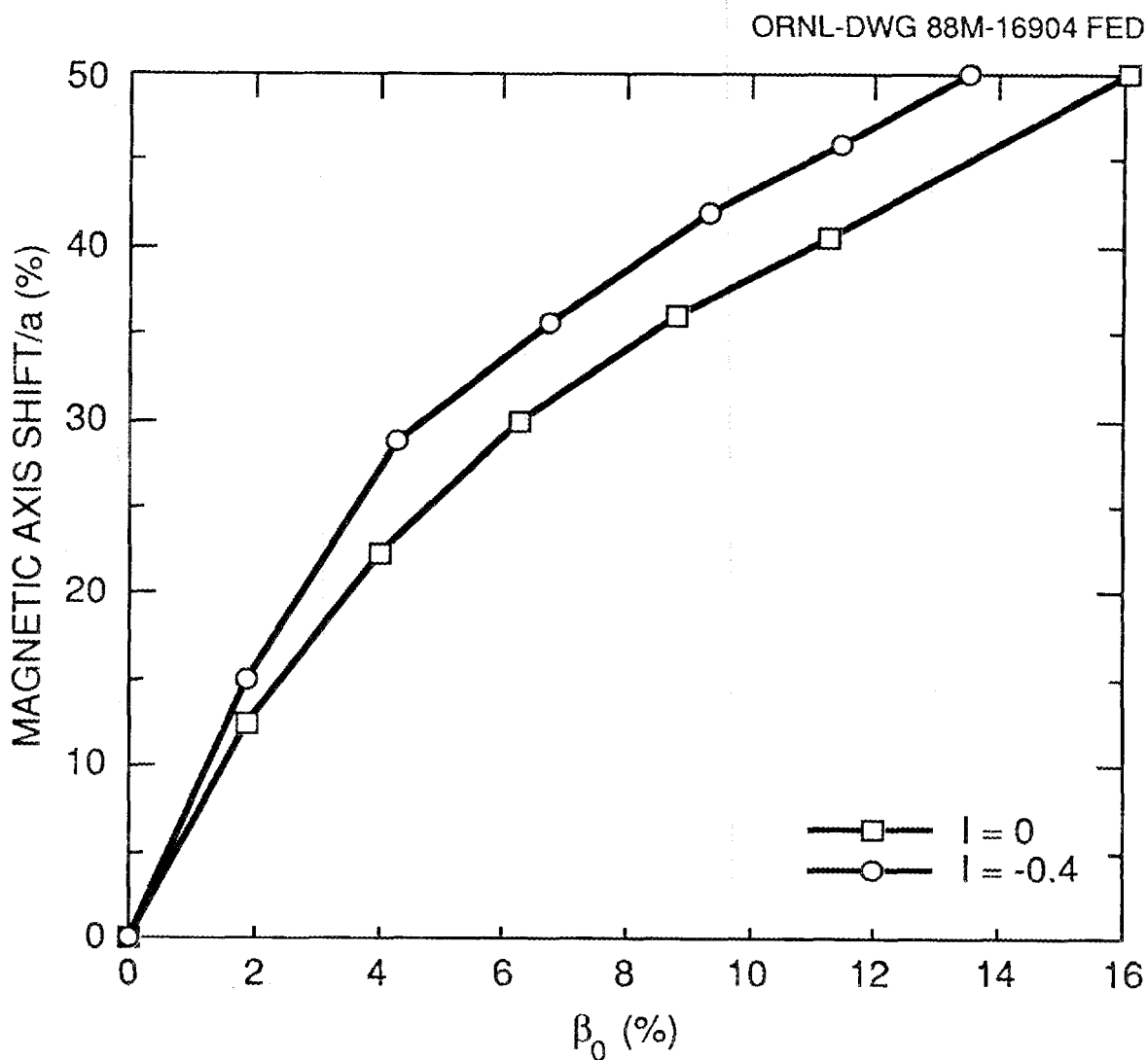


FIG. 10. Magnetic axis shift with beta for the CT9 configuration with (circles) and without (squares) an additional quadrupole field.

ORNL-DWG 89-16310 FED

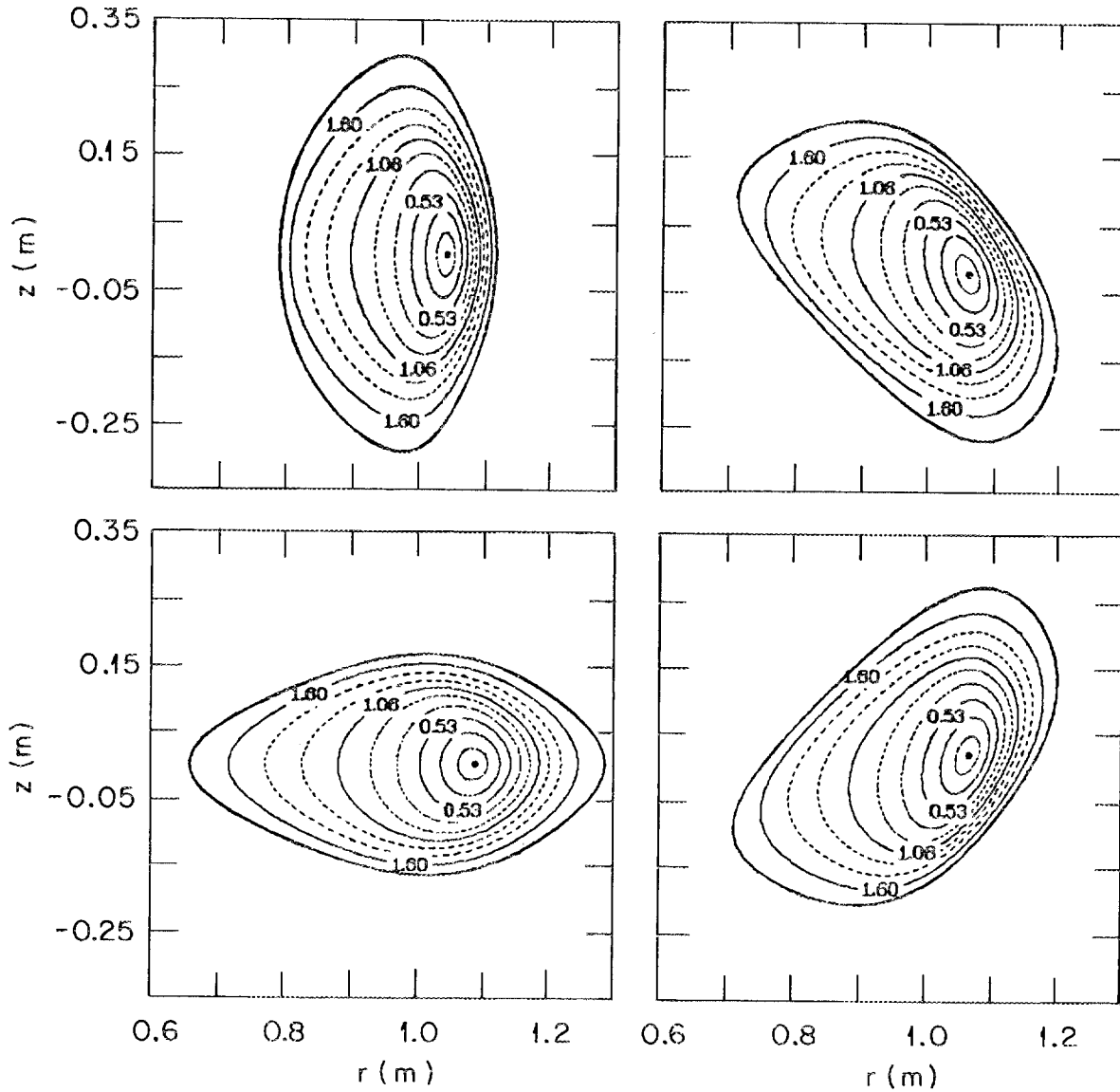


FIG. 11. Magnetic flux surfaces for a $\beta_0 = 4.3\%$ equilibrium calculated with the VMEC code for the CT9 configuration with an added quadrupole field ($I = -0.4$).

5. DISCUSSION AND CONCLUSIONS

From the results presented here, it is clear that simultaneous improvements in the MHD and transport properties of low-aspect-ratio torsatrons are possible. Configurations with aspect ratios in the range from 3.5 to 5 can be found with physics properties similar to those of ATF ($A_p = 7.8$). This improvement is real at low beta. However, as beta increases, the minimum- B contours are distorted, as shown in Fig. 12 for the CT7 configuration, and the energetic particle confinement

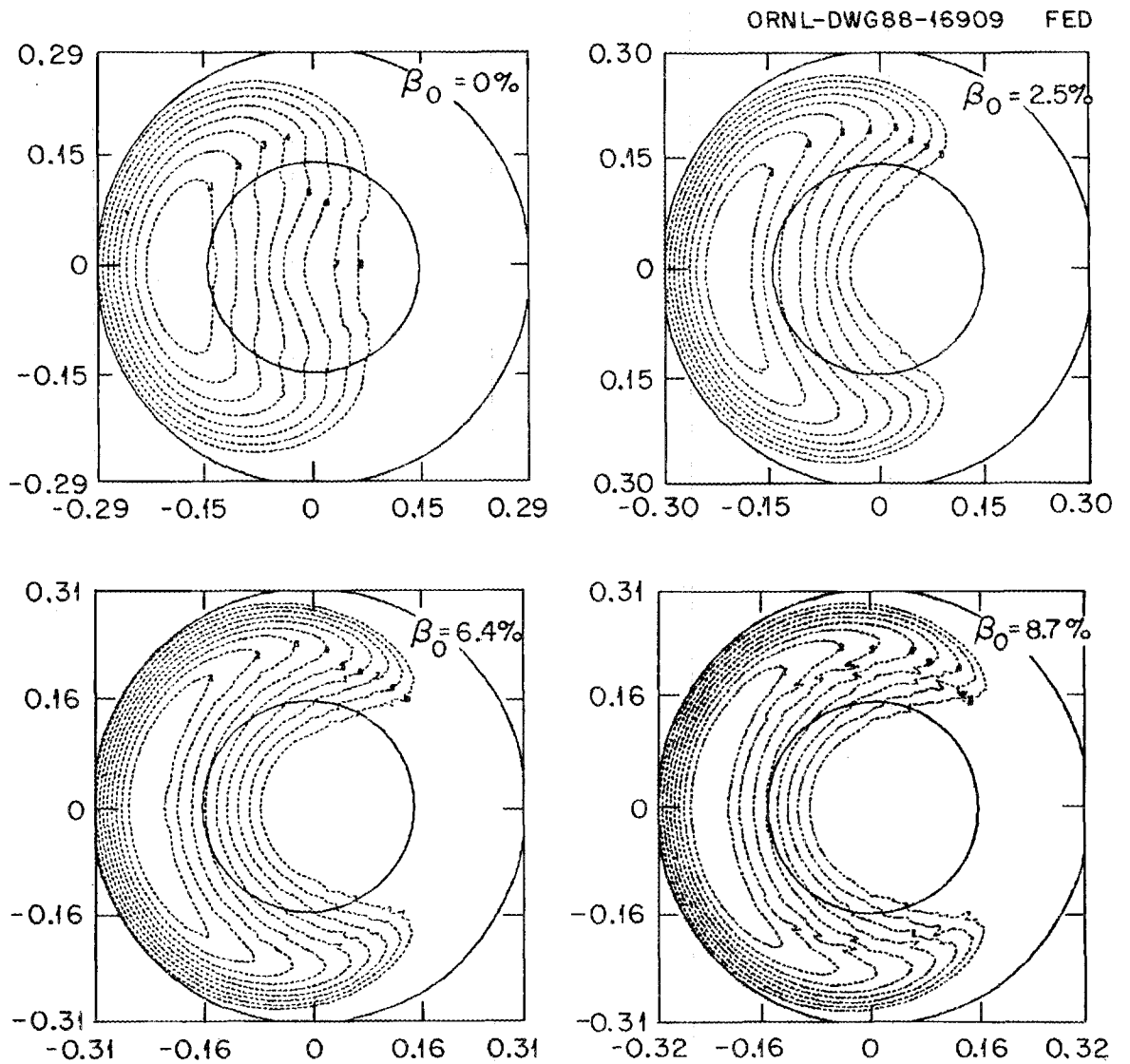


FIG. 12. Effect of beta on the minimum- B contours for the CT7 configuration with an added quadrupole field.

probably deteriorates in the inner plasma region. This is a consequence of the large shift of the magnetic axis with beta that is needed for the stability of the configuration. The value of A_B does not practically change with beta, but the strong distortion of the contours is a concern for alpha particle confinement. It is also important to notice that the results shown in Fig. 12 are from a 3-D fixed-boundary calculation using the VMEC code and that the minimum- B contours are crowding together at the inside boundary. Small changes in the plasma boundary have an important impact on the confinement of energetic particles, and how the plasma boundary will change with beta is one of the most difficult questions to answer for these configurations.

For the further development of low-aspect-ratio torsatrons, there are several outstanding needs:

1. Demonstrations of active control of magnetic surfaces and determination of how the outermost flux surfaces change with beta under such schemes. A new experiment is needed to resolve this issue.
2. A test of the reliability and completeness of the criteria used in the optimization. ATF should be able to address this issue.
3. Determination of the best compromise between the large shifts in magnetic axis needed for beta self-stabilization and adequate confinement of energetic particles in the plasma core. Resolving this issue will probably require the development of an alternative optimization approach.¹¹

ACKNOWLEDGMENT

We are grateful to S. P. Hirshman for making available the VMEC code for the calculation of 3-D equilibria.

REFERENCES

1. J. F. Lyon et al., "The Advanced Toroidal Facility," *Fusion Technol.* **10**, 179 (1986).
2. A. P. Navarro et al., "Configuration Studies for the TJ-II Device," p. 563 in *Proceedings of the 5th International Stellarator Workshop, Schloss Ringberg, 1984*, Vol. II, EUR9618 EN, Commission of the European Communities, Brussels, 1985.
3. M. Fujiwara et al., p. 288 in *Proceedings of the International Stellarator/Heliotron Workshop (Kyoto, 1986)*, Vol. II, PPLK-6, Kyoto University, Kyoto, Japan, 1987.
4. B. A. Carreras et al., "Low-Aspect-Ratio Torsatron Configurations," *Nucl. Fusion* **28**, 1195 (1988).
5. I. S. Danilkin, O. I. Fedyanin, I. S. Shpigel, and L. M. Kovrizhnykh, "Status and Initial Experimental Program of L-2M Stellarator," presented at the U.S.-U.S.S.R. Exchange II.4, Topical Meeting on Magnetic Configurations, Plasma Equilibrium, and Stability of Stellarators, Oak Ridge, Tennessee, June 23--July 3, 1986.
6. B. A. Carreras et al., "Low-Aspect-Ratio Torsatrons," presented at the 12th International Conference on Plasma Physics and Controlled Nuclear Fusion Research, Nice, France, 1988 (proceedings to be published by the International Atomic Energy Agency, Vienna).
7. V. E. Bykov, E. D. Volkov, A. B. Georgievskii, Yu. K. Kuznetsov, S. A. Martynov, V. G. Peletninskaya, K. S. Rubtsev, V. A. Rudakov, Yu. F. Sergeev, A. V. Khodyachikh, and A. A. Shiskin, "Optimization Studies of Compact Torsatrons," presented at the 12th International Conference on Plasma Physics and Controlled Nuclear Fusion Research, Nice, France, 1988 (proceedings to be published by the International Atomic Energy Agency, Vienna).
8. J. Sheffield et al., "Cost Assessment of a Generic Fusion Reactor," *Fusion Technol.* **9**, 199 (1986).
9. J. F. Lyon, B. A. Carreras, V. E. Lynch, J. S. Tolliver, and I. N. Sviatoslavsky, "Compact Torsatron Reactors," *Fusion Technol.*, accepted for publication (1989); also published as ORNL/TM-10572 (1988).
10. J. R. Cary and J. D. Hanson, *Phys. Fluids* **29**, 2464 (1986).
11. S. P. Hirshman et al., "Studies Relating to Optimization of Low-Aspect-Ratio Stellarators," to be presented at the 7th International Stellarator Workshop, Oak Ridge, Tennessee, April 10-14, 1989 (proceedings to be published by IAEA).

12. A. H. Reiman and A. H. Boozer, *Phys. Fluids* **27**, 2446 (1984).
13. K. Miyamoto, *Plasma Physics for Nuclear Fusion*, MIT Press, Cambridge, Mass., 1976.
14. K. C. Shaing and S. A. Hokin, "Neoclassical Transport in a Multiple Helicity Torsatron in the Low Collisionality ($1/\nu$) Regime," *Phys. Fluids* **26**, 2136 (1983).
15. S. L. Painter and J. F. Lyon, "Alpha Particle Losses in Compact Torsatron Reactors," *Fusion Technol.*, accepted for publication (1989).
16. A. M. Boozer, *Phys. Fluids* **25**, 520 (1982).
17. C. L. Hedrick, Oak Ridge National Laboratory, private communication, 1989.
18. K. C. Shaing and J. D. Callen, "Calculation of the Parallel Viscosity in the Plateau Regime," *Phys. Fluids* **26**, 1526 (1983).
19. K. C. Shaing, B. A. Carreras, N. Dominguez, V. E. Lynch, and J. S. Tolliver, "Bootstrap Current Control in Stellarators," *Phys. Fluids B*, accepted for publication (1989).
20. L. M. Kovrizhnykh and S. V. Shchepetov, *Sov. J. Plasma Phys.* **7**, 229 (1981).
21. C. Mercier, *Nucl. Fusion* **1**, 47 (1960).
22. S. P. Hirshman, W. I. van Rij, and P. Merkel, "Three-Dimensional Free-Boundary Calculation Using a Spectral Green's Function Method," *Comput. Phys. Comm.* **43**, 143 (1986).

ORNL/TM-11101

Dist. Category UC-427

INTERNAL DISTRIBUTION

- | | | | |
|--------|-----------------|--------|---|
| 1. | D. B. Batchelor | 32. | J. A. Rome |
| 2-6. | B. A. Carreras | 33. | K. C. Shaing |
| 7. | M. D. Carter | 34. | J. Sheffield |
| 8. | E. C. Crume | 35. | D. A. Spong |
| 9-13. | N. O. Dominguez | 36-37. | Laboratory Records Department |
| 14. | R. A. Dory | 38. | Laboratory Records, ORNL-RC |
| 15. | C. L. Hedrick | 39. | Document Reference Section |
| 16. | S. P. Hirshman | 40. | Central Research Library |
| 17. | J. T. Hogan | 41. | Fusion Energy Division Library |
| 18. | W. A. Houlberg | 42-43. | Fusion Energy Division
Publications Office |
| 19. | H. C. Howe | 44. | ORNL Patent Office |
| 20. | E. F. Jaeger | | |
| 21-25. | J-N. Leboeuf | | |
| 26. | G. S. Lee | | |
| 27-31. | J. F. Lyon | | |

EXTERNAL DISTRIBUTION

45. Office of the Assistant Manager for Energy Research and Development, U.S. Department of Energy, Oak Ridge Operations Office, P. O. Box E, Oak Ridge, TN 37831
46. J. D. Callen, Department of Nuclear Engineering University of Wisconsin Madison, WI 53706-1687
47. J. F. Clarke, Director, Office of Fusion Energy, Office of Energy Research, ER-50 Germantown, U.S. Department of Energy, Washington, DC 20545
48. R. W. Conn, Department of Chemical, Nuclear, and Thermal Engineering, University of California, Los Angeles, CA 90024
49. S. O. Dean, Fusion Power Associates, 2 Professional Drive, Suite 248, Gaithersburg, MD 20879
50. H. K. Forsen, Bechtel Group, Inc., Research Engineering, P. O. Box 3965, San Francisco, CA 94105
51. J. R. Gilleland, L-644, Lawrence Livermore National Laboratory, P.O. Box 5511, Livermore, CA 94550
52. R. W. Gould, Department of Applied Physics, California Institute of Technology, Pasadena, CA 91125
53. R. A. Gross, Plasma Research Laboratory, Columbia University, New York, NY 10027
54. D. M. Meade, Princeton Plasma Physics Laboratory, P.O. Box 451, Princeton, NJ 08544
55. M. Roberts, International Programs, Office of Fusion Energy, Office of Energy Research, ER-52 Germantown, U.S. Department of Energy, Washington, DC 20545
56. W. M. Stacey, School of Nuclear Engineering and Health Physics, Georgia Institute of Technology, Atlanta, GA 30332

57. D. Steiner, Nuclear Engineering Department, NES Building, Tibbetts Avenue, Rensselaer Polytechnic Institute, Troy, NY 12181
58. R. Varma, Physical Research Laboratory, Navrangpura, Ahmedabad 380009, India
59. Bibliothek, Max-Planck Institut für Plasmaphysik, Boltzmannstrasse 2, D-8046 Garching, Federal Republic of Germany
60. Bibliothek, Institut für Plasmaphysik KFA Jülich GmbH, Postfach 1913, D-5170 Jülich, Federal Republic of Germany
61. Bibliothek, KfK Karlsruhe GmbH, Postfach 3640, D-4500 Karlsruhe 1, Federal Republic of Germany
62. Bibliotheque, Centre de Recherches en Physique des Plasmas, 21 Avenue des Bains, CH-1007 Lausanne, Switzerland
63. R. Aymar, CEN/Cadarache, Departement de Recherches sur la Fusion Contrôlée, F-13108 Saint-Paul-lez-Durance Cedex, France
64. Bibliothèque, CEN/Cadarache, F-13108 St.-Paul-lez-Durance, Cedex, France
65. Library, Culham Laboratory, UKAEA, Abingdon, Oxfordshire, OX14 3DB, England
66. Library, JET Joint Undertaking, Abingdon, Oxfordshire, OX14 3EA, England
67. Library, FOM-Instituut voor Plasma-Fysica, Rijnhuizen, Edisonbaan 14, 3439 MN Nieuwegein, The Netherlands
68. Library, Institute of Plasma Physics, Nagoya University, Nagoya 464, Japan
69. Library, International Centre for Theoretical Physics, P.O. Box 586, I-34100 Trieste, Italy
70. Library, Centro Recherche Energia Frascati, C.P. 65, I-00044 Frascati (Roma), Italy
71. Library, Plasma Physics Laboratory, Kyoto University, Gokasho, Uji, Kyoto 611, Japan
72. Plasma Research Laboratory, Australian National University, P.O. Box 4, Canberra, A.C.T. 2601, Australia
73. Library, Japan Atomic Energy Research Institute, Naka Fusion Research Establishment, 801-1 Mukoyama, Naka-machi, Naka-gun, Ibaraki-ken, Japan
74. G. A. Eliseev, I. V. Kurchatov Institute of Atomic Energy, P.O. Box 3402, 123182 Moscow, U.S.S.R.
75. V. A. Glukhikh, Scientific-Research Institute of Electro-Physical Apparatus, 188631 Leningrad, U.S.S.R.
76. I. Shpigel, Institute of General Physics, U.S.S.R. Academy of Sciences, Ulitsa Vavilova 38, Moscow, U.S.S.R.
77. D. D. Ryutov, Institute of Nuclear Physics, Siberian Branch of the Academy of Sciences of the U.S.S.R., Sovetskaya St. 5, 630090 Novosibirsk, U.S.S.R.
78. V. T. Tolok, Kharkov Physical-Technical Institute, Academical St. 1, 310108 Kharkov, U.S.S.R.
79. Deputy Director, Southwestern Institute of Physics, P.O. Box 15, Leshan, Szichuan, China (PRC)
80. Director, Institute of Plasma Physics, P.O. Box 26, Hefei, Anhui, China (PRC)
81. D. Crandall, Experimental Plasma Research Branch, Division of Development and Technology, Office of Fusion Energy, Office of Energy Research, ER-542 Germantown, U.S. Department of Energy, Washington, DC 20545
82. N. A. Davies, Office of the Associate Director, Office of Fusion Energy, Office of Energy Research, ER-51 Germantown, U.S. Department of Energy, Washington, DC 20545
83. R. H. McKnight, Experimental Plasma Research Branch, Division of Development and Technology, Office of Fusion Energy, Office of Energy Research, ER-51 Germantown, U.S. Department of Energy, Washington, DC 20545

84. D. B. Nelson, Director, Division of Applied Plasma Physics, Office of Fusion Energy, Office of Energy Research, ER-54 Germantown, U.S. Department of Energy, Washington, DC 20545
85. E. Oktay, Division of Confinement Systems, Office of Fusion Energy, Office of Energy Research, ER-55 Germantown, U.S. Department of Energy, Washington, DC 20545
86. W. Sadowski, Fusion Theory and Computer Services Branch, Division of Applied Plasma Physics, Office of Fusion Energy, Office of Energy Research, ER-541 Germantown, U.S. Department of Energy, Washington, DC 20545
87. R. E. Mickens, Atlanta University, Department of Physics, Atlanta, GA 30314
88. M. N. Rosenbluth, University of California at San Diego, La Jolla, CA 92093
89. Duk-In Choi, Department of Physics, Korea Advanced Institute of Science and Technology, P.O. Box 150, Chong Ryang-Ri, Seoul, Korea
90. Library of the Physics Department, University of Ioannina, Ioannina, Greece
91. C. De Palo, Library, Associazione EURATOM-ENEA sulla Fusione, C.P. 65, Frascati (Roma), Italy
92. Theory Department Read File, c/o D. W. Ross, University of Texas, Institute for Fusion Studies, Austin, TX 78712
93. Theory Department Read File, c/o R. Parker, Director, Plasma Fusion Center, NW 16-202, Massachusetts Institute of Technology, Cambridge, MA 02139
94. Theory Department Read File, c/o R. White, Princeton Plasma Physics Laboratory, P.O. Box 451, Princeton, NJ 08544
95. Theory Department Read File, c/o L. Kovrizhnykh, Lebedev Institute of Physics, Academy of Sciences, 53 Leninsky Prospect, 117924 Moscow, U.S.S.R.
96. Theory Department Read File, c/o B. B. Kadomtsev, I. V. Kurchatov Institute of Atomic Energy, P.O. Box 3402, 123182 Moscow, U.S.S.R.
97. Theory Department Read File, c/o T. Kamimura, Institute of Plasma Physics, Nagoya University, Nagoya 464, Japan
98. Theory Department Read File, c/o C. Mercier, Departement de Recherches sur la Fusion Contrôlée, B.P. 6, F-92260 Fontenay-aux-Roses (Seine), France
99. Theory Department Read File, c/o T. E. Stringer, JET Joint Undertaking, Culham Laboratory, Abingdon, Oxfordshire OX14 3EA, England
100. Theory Department Read File, c/o R. Briscoe, Culham Laboratory, Abingdon, Oxfordshire OX14 3DB, England
101. Theory Department Read File, c/o D. Biskamp, Max-Planck-Institut für Plasmaphysik, Boltzmannstrasse 2, D-8046 Garching, Federal Republic of Germany
102. Theory Department Read File, c/o T. Takeda, Japan Atomic Energy Research Institute, Tokai Establishment, Tokai-mura, Naka-gun, Ibaraki-ken, Japan
103. Theory Department Read File, c/o J. Greene, General Atomics, P.O. Box 81608, San Diego, CA 92138
104. Theory Department Read File, c/o L. D. Pearlstein, L-630, Lawrence Livermore National Laboratory, P.O. Box 5511, Livermore, CA 94550
105. Theory Department Read File, c/o R. Gerwin, CTR Division, Los Alamos National Laboratory, P.O. Box 1663, Los Alamos, NM 87545
106. J. L. Johnson, Plasma Physics Laboratory, Princeton University, P.O. Box 451, Princeton, NJ 08543
107. O. Motojima, Plasma Physics Laboratory, Kyoto University, Gokasho, Uji, Kyoto, Japan
108. D. Schnack, SAIC, 10260 Campus Point Drive, San Diego, CA 92121
109. V. D. Shafranov, I. V. Kurchatov Institute of Atomic Energy, P.O. Box 3402, 123182 Moscow, U.S.S.R.
110. J. L. Shohet, Torsatron/Stellarator Laboratory, University of Wisconsin, Madison, WI 53706

111. H. Wobig, Max-Planck-Institut für Plasmaphysik, Boltzmannstrasse 2, D-8046 Garching, Federal Republic of Germany
- 112-157. Given distribution according to OSTI-4500, Magnetic Fusion Energy (Category Distribution UC-427, Theoretical Plasma Physics)